



Trans. Nonferrous Met. Soc. China 31(2021) 2062-2073

Transactions of Nonferrous Metals Society of China

www.tnmsc.cn



Enhancing electrochemical performance of SnO₂ anode with humic acid modification

Shu-zhen YANG, Yan-fang HUANG, Xue-chun HAN, Gui-hong HAN
School of Chemical Engineering, Zhengzhou University, Zhengzhou 450001, China
Received 31 July 2020; accepted 28 January 2021

Abstract: Humic acid (HA) was studied as a modifier in the SnO₂ anode preparation for the electrochemical performance improvement. Scanning electron microscopy, 180° peel test, and nanoindentation experiment were used to examine the influence of the HA on electrode. The results showed that the addition of HA could improve the dispersion uniformity of all particles. The components were tightened, increasing the difficulty of peeling off the film from the current collector. The deformation resistance of the electrode was greatly enhanced by the HA modification. The electrochemical test results showed that the anode from the normal micron-sized SnO₂ particles with the HA modifier exhibited significant progress in electrochemical performance compared with those without HA. The reversible specific capacity of the SnO₂ anode can be maintained as high as 733.4 mA·h/g at a current density of 100 mA/g after 50 cycles. Therefore, HA is a promising modifier for anode preparation of lithium-ion batteries.

Key words: SnO₂ anode; humic acid; electrode modification; lithium-ion batteries

1 Introduction

Lithium-ion batteries (LIBs) are widely applied nowadays, from cars to microchips [1]. The performance requirement for LIBs is progressively increasing as the society develops, and the traditional graphite anode material cannot satisfy the demand because it is limited by its low theoretical specific capacity. Thus, new materials with a high specific capacity have been proposed, such as Si, Sn, and some metallic oxides [2-6]. Among them, SnO₂ is one of the most promising candidate anode materials applied in LIBs and has been widely studied due to its high theoretical specific capacity (782 mA·h/g) and availability. Nevertheless, the volume change of the material during the charge-discharge process can lead to the cementing action between the material and the binder invalidation and further result in the structure collapse of the entire coating section. The cycle stability can be dramatically affected if the active material cannot connect well with the entire conductive system of the electrode. Thus, this problem needs to be solved with great urgency to obtain high-performance LIBs.

Considerable efforts and resources have been devoted to improving the electrochemical performance of SnO₂. So far, two main directions have been followed, namely, changing the structure and morphology of the active material, and applying a functional binder, to accommodate the volume change. Most researchers focused on the morphology and structure design, and many promising materials have been fabricated in the past several years. Regulating the particle size to nano-grade is an effective method of alleviating volume variation [7–9]. A porous or hollow structure can reserve a space for volume variation and hence achieve excellent performance [10–12].

However, the tedious preparation process of these materials can limit their industrialization. The binder, a small proportion contained in electrode, has a considerable influence on batteries [13,14]. Polyvinylidene fluoride (PVDF), a widely used binder in anode preparation, is expensive and must usually be dissolved in the toxic and organic combustible solvent N-methyl-2pyrrolidone (NMP) [15,16]. It cannot buffer the volume change from electrode materials during the charge-discharge process and thus may not prevent the pulverization of materials [17]. Some novel binders for the SnO₂ anode have been reported, such as sodium carboxymethyl cellulose (CMC) [18-22], poly(acrylic acid) (PAA) [23], Na-lignite [22,24], CMC and styrene-butadiene rubber [25], and the cross-linked binder formed by PAA and soluble starch [26]. Among them, CMC has been widely studied because of its polyethylene backbone that implies high flexibility. In the dried and bulk state, CMC shows a high elastic modulus because of the intermolecular hydrogen bonding between the side groups [27]. However, deep cracks usually appear on the electrode surface [28], which may be attributed to the rigid molecular structure of the CMC caused by the nature of the pyranose linkages. The cracks in the electrode go against the stable presence of active materials on the electrode surface and can reduce the charge transfer efficiency. To address this problem, an effective component must be developed to modify the electrode.

Humic acid (HA) is a moderate polyelectrolyte with different organic functional groups [29-31] and possesses a loose structure. It can be taken as a precursor to obtain the graphene oxide-like nanosheets [32]. In a previous study [29], HA was selected as the anode material for LIBs and displayed a satisfactory performance. Considering the properties of coagulation, gelation, and dispersion, HA might be a good candidate for modifying the electrode surface and consequently enhancing the conductivity of the electrode for further electrochemical performance improvement. However, few studies have reported the conception of the modifier for anode improvement. Herein, HA was creatively taken as the anode modifier from a novel perspective.

In this work, a characterless SnO₂ obtained through a simple calcination method was selected

to prove the robustness of the modifier. The water-soluble binder CMC was used for electrode preparation. The electrodes from the regular binder of CMC and PVDF without a modifier were studied for comparison. The anode characteristics, including surface morphology, film adhesion, and deformation resistance, were investigated to show the advantage of the HA modifier. The electrochemical performance of different anodes was compared and discussed in detail. This work developed a new approach for anode performance optimization.

2 Experimental

2.1 Materials

The reagents for SnO₂ synthesis mainly include SnCl₂·2H₂O (GR grade, Tianjin Kemiou Chemical Reagent Co., Ltd., China) and sorbate-80 (AR grade, Fengchuan Chemical Reagent Co., Ltd., China). SnO₂ was synthesized as follows. Typically, 60 mL of SnCl₂ solution with a concentration of 0.45 mol/L was mixed with 3 mL of sorbate-80. Then, the mixture was stirred intensely for 30 min in a water bath at 60 °C. Afterward, 60 mL of (NH₄)₂CO₃ solution with a concentration of 0.45 mol/L was dropwise added in the system. After 30 min of continuous, intense stirring at 60 °C, the pH of the solution was adjusted to ~10 with a 2 mol/L NaOH solution. The system temperature was increased to 80 °C in a water bath, and then the solution was stirred for 1 h. Then, the precipitate was collected by centrifugal washing several times. The powder was collected by vacuum drying at 60 °C for 24 h. Finally, the product was obtained by calcination in a tube furnace at 350 °C for 3 h in air. HA (fulvic acid ≥90%) was purchased from Aladdin Industrial Co., Ltd., China. Sodium carboxymethyl cellulose (CMC, AR) was acquired from the Dow Chemical Company. All chemical reagents were used as received without further purification.

The HA used in this work is not a pure substance and cannot be defined by a definite molecular formula. The chemical bonds in the HA were characterized by Fourier transform-infrared (FT-IR) instrument (Fig. 1). The peak located at 3367 cm⁻¹ is due to the stretching vibration of O—H, and the peak located at 1654 cm⁻¹ is derived from the C—N stretching vibration of the amide I band and the stretching vibration from quinone

C=O and/or the C=O of the H-bonded conjugated ketones. The peak at 1560 cm⁻¹ is assigned to the symmetric stretching vibration of COO⁻, the bending vibration of N—H, and the stretching vibration of the C=N of the amide II band. The peak positioned at 1028 cm⁻¹ belongs to the C—O stretching vibration of the polysaccharide or polysaccharide-substance, and Si—O of the silicate impurities [33].

The surface morphology of HA was observed by scanning electron microscopy (SEM) and transmission electron microscopy (TEM) (Fig. 2). HA has no definite shape (Fig. 2(a)) and thus can be a good dispersion medium for particles of active

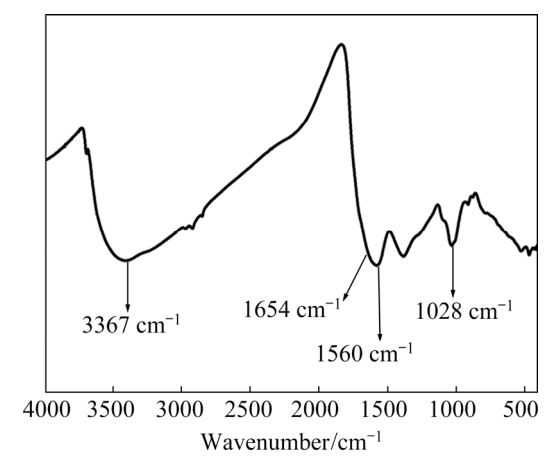


Fig. 1 FT-IR spectrum of HA

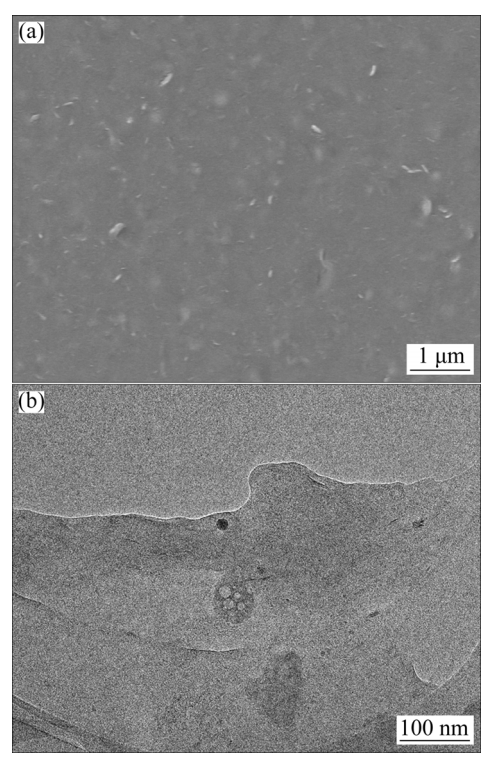


Fig. 2 SEM (a) and TEM (b) images of HA

material and conductive reagent. The HA surface has some flaky textures. The flakes are quite thin, with nanoscale thicknesses (Fig. 2(b)) and can thus be good buffering objects. The morphology characteristic of HA may enhance the adhesion of electroactive materials with current collector [34].

2.2 Characterization

The crystal structure of SnO₂ was characterized by X-ray diffractometry (XRD, Bruker D8Advance). The vibration modes of the key groups of SnO₂ and HA were investigated by FT-IR instrument (Nicolet iS10) using the KBr pellet. The morphologies of the synthesized SnO₂, HA, and the SnO₂ electrodes were characterized by ZEISS Auriga FIB-SEM, TEM (FEI TalosF 200S) and atomic force microscopy (AFM, JPK NanoWizard®, Bruker Nano GmbH, Germany). The Brunauer-Emmett-Teller method (BET, Micromeritics ASAP 2460) was used to measure the specific surface area and pore size distribution of SnO2. The adhesion strength between the film and the current collector was measured by means of the 180° peel test using the method reported by WEI et al [35]. Nanoindentation experiments were performed with a nano indenter G200 (America). The surface approach velocity was maintained at 10 nm/s during the measurement. A diamond Berkovich indenter was forced into the tested object, while the force and the indentation depth were continuously recorded. Ten tests were conducted for each testing condition to obtain statistically significant data sets.

2.3 Electrochemical measurements

The control electrode was composed of the binder, the conductive agent of acetylene black, and the prepared SnO₂ material at a mass ratio of 1:1:8. The modification electrode was composed of the binder, the HA modifier, the conductive agent of acetylene black, and the prepared SnO2 material at a mass ratio of 1:1:2:16. The binder, the modifier, and the conductive agent were added into the solvent (HA and CMC corresponding to water and PVDF corresponding to NMP) in sequence while stirring for 1 h. Then, SnO₂ powder was mixed with them while continuously stirring until the slurry became homogenous. Subsequently, the slurry was cast on a copper foil with an automatic doctor blade, followed by drying at 60 °C for 2 h in an electric blast drying oven. Finally, the sheet was thoroughly

dried at 60 °C under vacuum atmosphere overnight. The sheet was cut into wafers with a diameter of 8 mm. The active material loading for every anode was approximately 1.6 mg/cm². The lithium metal disc was taken as the reference electrode, and Celgard 2500 was used as the cell separator. The electrolyte was 1 mol/L LiPF₆ dissolved in ethylene carbonate/ethyl methyl carbonate/dimethyl carbonate (1:1:1, volume ratio). The electrochemical performance was observed through CR2032 coin-type cells, which were assembled in an argon-filled glove box.

Cyclic voltammetry (CV) and electrochemical impedance spectroscopy measurements were taken using an Autolab PGSTAT204 (Holland) electrochemical working station. Galvanostatic charge–discharge tests were performed on the LAND system in the potential range of 0.05–2.5 V (vs Li/Li⁺). All the tests were carried out at 25 °C.

3 Results and discussion

3.1 SnO₂ and electrode characterization

The XRD pattern in Fig. 3 shows that the product is pure tetragonal cassiterite, SnO_2 , because all the peaks are well-indexed to the peaks in JCPDS No. 41-1445. The crystallite size of SnO_2 (*D*) was estimated by the major diffraction peaks of (110) by the Scherrer equation [36] (Eq. (1)):

$$D = \frac{K\lambda}{\beta\cos\theta} \tag{1}$$

where β is the breadth of the diffraction line at its half intensity. θ is the Bragg angle. K is the shape factor, which usually takes a value of approximately 0.89. λ is the wavelength of the X-ray source used

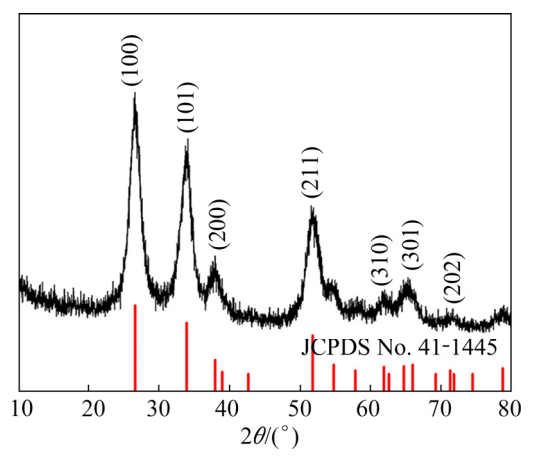


Fig. 3 XRD pattern of SnO₂

in XRD measurement, which is 1.5406 nm. The calculated crystalline domain size is 58 nm for SnO₂.

The FT-IR spectrum of SnO₂ is shown in Fig. 4. The peaks at 3441 and 1635 cm⁻¹ are respectively derived from the stretching and bending vibrations of the O—H bond from the H₂O absorbed on SnO₂, and the peak at 624 cm⁻¹ is ascribed to the antisymmetric vibration of the O—Sn—O bonds [8].

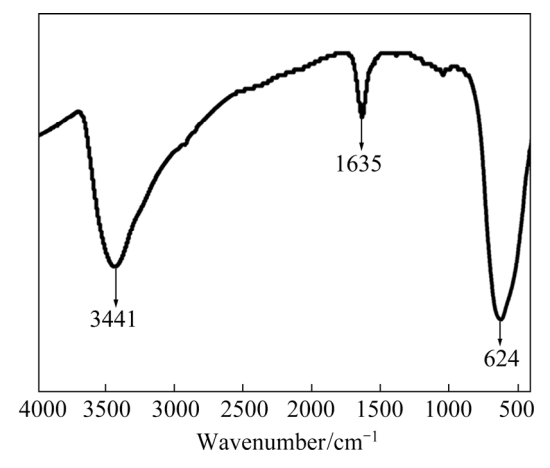


Fig. 4 FT-IR spectrum of SnO₂

The morphology of the as-prepared SnO₂ was observed by SEM. Figure 5(a) shows that the average diameter of the particles is approximately 0.5 µm. The irregular spherical particles with rough surfaces were observed in a higher magnification (Fig. 5(b)). The large particles in microscale (Fig. 5(a)) are composed of many nanoparticles (Fig. 5(b)). The specific surface area of SnO₂ is $78.4 \text{ m}^2/\text{g}$ from the BET test. The N₂ adsorption and desorption curves are presented in Fig. 6(a). The typical IV type curve of the mesoporous structure can be observed [37]. The adsorption hysteresis at P/P_0 of 0.4–0.8 was probably caused by the capillary condensation during the desorption process [38]. The pore size distribution of SnO₂ obtained by the Barrett-Joyner-Halenda method is shown in Fig. 6(b), and the pore diameter is concentrated at 3.4 nm.

The surfaces of the SnO₂ electrode with different compositions were observed by SEM and AFM. The electrode with HA-CMC (Figs. 7(a, b)) is the most uniform among the three electrodes (Figs. 7(a-f)). The SnO₂ particles are more homogenously distributed because of good dispersion effect of HA. In comparison, the surface

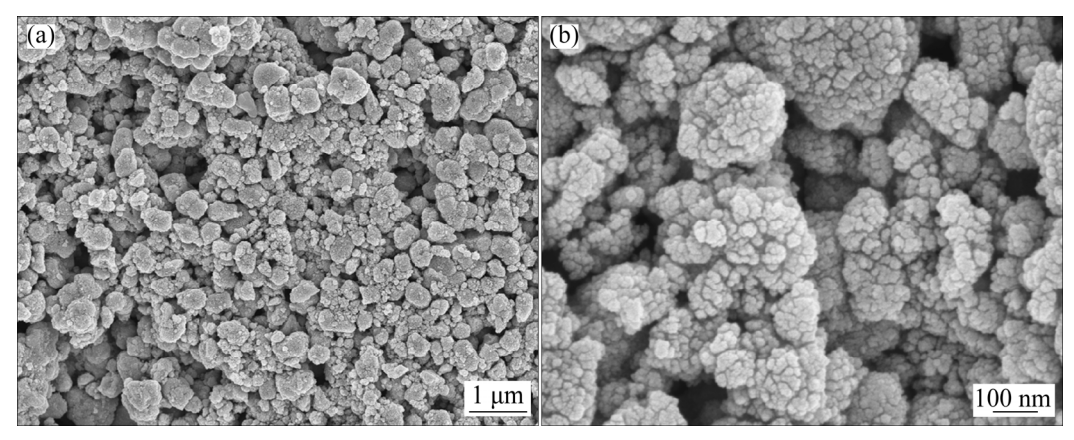


Fig. 5 SEM images of SnO₂: (a) Lower magnification; (b) Higher magnification

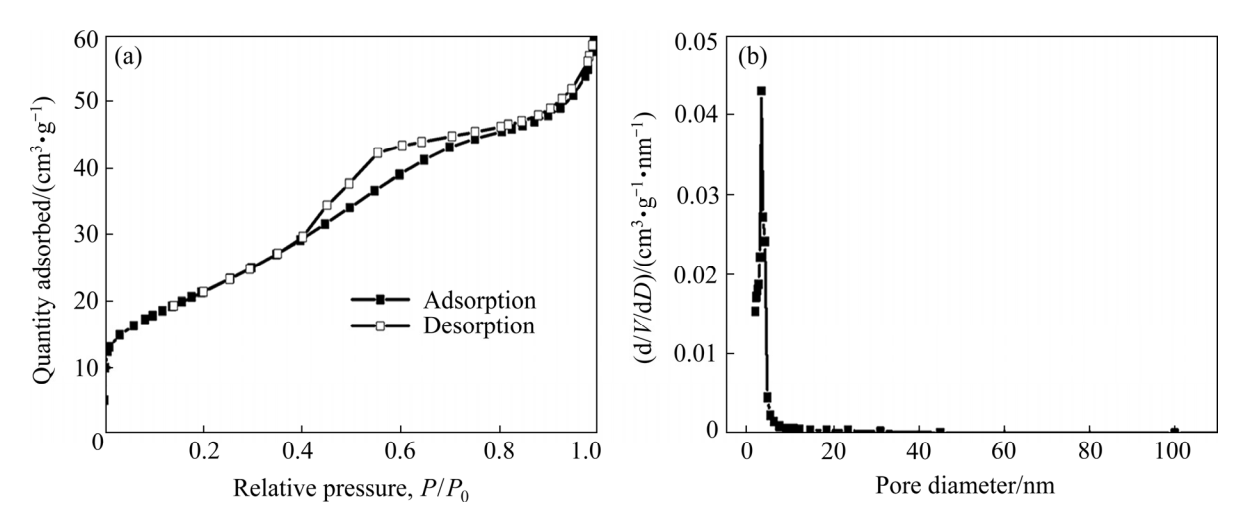


Fig. 6 N₂ adsorption–desorption curves (a) and pore size distribution (b) of SnO₂

of the electrodes with PVDF seems to be smooth overall (Fig. 7(c)), while obvious cracks are observed in a higher magnification, and the distributions of different components are discrete (see the dashed circled lines in Fig. 7(d)). Cracks are easily formed in the aggregate areas of the SnO₂ particles, which may impede the transportation of Li ions. The electrode with CMC alone as binder has a rough surface and many cracks (Figs. 7(e, f)). This phenomenon is mainly caused by the effect of the strong cohesion from CMC. However, the existence of HA may greatly distract the force by forming hydrogen bonds with CMC and providing steric hindrance [39]. In addition, many small holes can be observed in the electrodes (Figs. 7(b, f)), providing extra passages for ion transportation and reserved space to buffer the volume effect during the charge and discharge processes. Consistent results were obtained by AFM (Figs. 7(g-i). The average roughness (Ra) values of the HA-CMC, PVDF, and CMC electrode surfaces are 106, 143.6,

and 187.9 nm, respectively. The low $R_{\rm a}$ value of the HA–CMC may be beneficial to elevating the initial efficiency, columbic efficiency (CE), discharge capacity, and capacity retention of lithium ion batteries [40]. The schematic diagram of the HA modification of the electrode surface is displayed in Fig. 8. The high flexibility of humic substances enables them to adapt well to the interaction between the active material, the conductive agent, and the companied binder. By adding HA, different compositions can be distributed on the copper foil with force balance to avoid cracks.

The adhesion strength of the material to the Cu current collector was evaluated by the 180° peeling test, and the results are illustrated in Fig. 9. Among the laminates tested, SnO₂–CMC and SnO₂–HA–CMC displayed higher adhesion strength than SnO₂–PVDF. SnO₂–HA–CMC exhibits the highest average peeling load of 0.82 N, indicating the reliable adhesion and relative stable state of the HA–CMC.

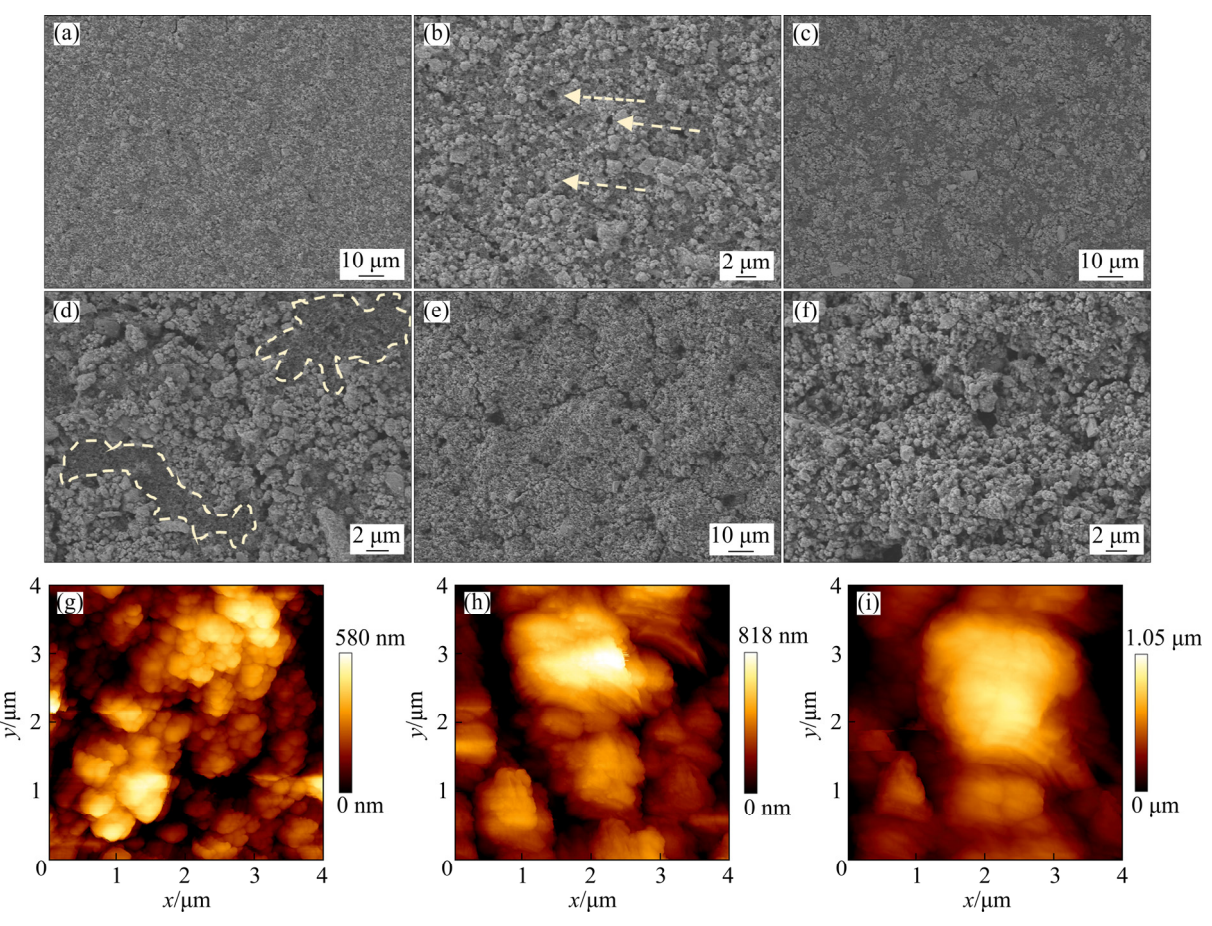


Fig. 7 SEM (a–f) and AFM (g–i) images of electrode surface with different compositions of HA–CMC (a, b, g), PVDF (c, d, h) and CMC (e, f, i)

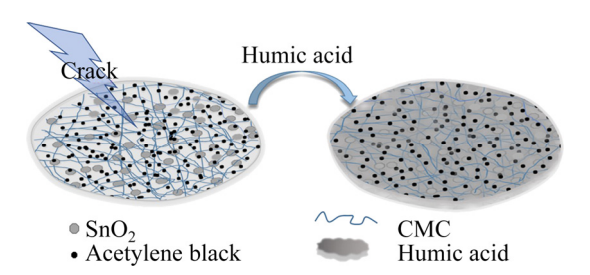


Fig. 8 Schematic diagram of HA modification for electrode surface

The mechanical properties of different SnO_2 electrodes with HA–CMC, PVDF, and CMC were assessed using the nanoindentation method. Figure 10 shows the nanoindentation process profiles of HA–CMC, PVDF, and CMC. The final depth (h_f), which is the residual depth of the hardness impression after the final unloading, represents the deformation after the nanoindentation process that is similar to expansion and contraction of the anode material in the electrode [28]. Apparently, HA–CMC has a higher deformation resistance to adapt to volume change.

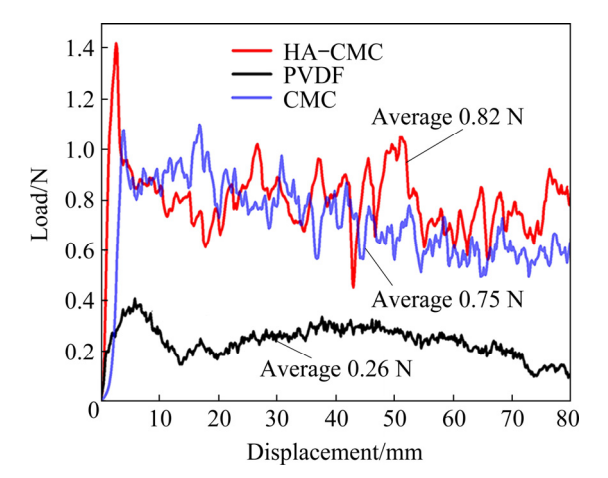


Fig. 9 180° peeling test results of different SnO_2 electrodes

3.2 Electrochemical performance

The CV curves were first compared among the three electrodes at a scan rate of 0.3 mV/s (Fig. 11). The irreversible reduction peaks ranging from 1.5 to 0.1 V in the first discharge are mainly due to the transformation of SnO_2 to Sn (Reaction (2)), the electrolyte decomposition on the electrode surface,

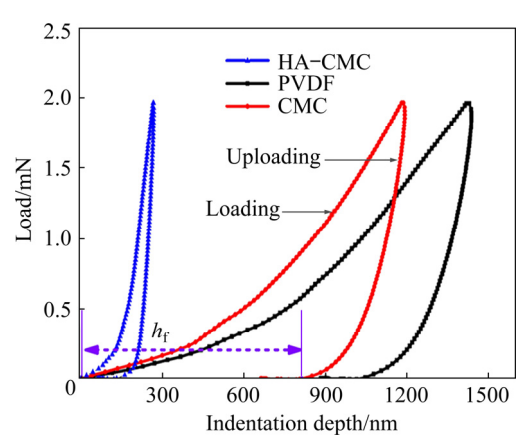


Fig. 10 Load-indentation depth curves of different SnO₂ electrodes

and the formation of solid electrode interface (SEI) (Reaction (3)) [10,41–43]. The reversible reduction peaks near 0 V are ascribed to the alloying process of Li⁺ (Reaction (4)). The reversible oxidation peaks around 0.6 V are from the reverse reaction of Reaction (4), which represents the lithium ion dealloying reaction. The oxidation peaks at 1.3 V in

the charge process correspond to the oxidation of Sn to SnO₂, indicating that Reaction (2) is partly reversible. The oxidation peaks from 1.80 to 2.20 V that only appear on the CMC and the HA-CMC CVs are probably attributed to the excess Li⁺ capacity to Li⁺ diffusion reversibly into/out the interior space of the HA-CMC-SnO₂ and CMC-SnO₂ electrodes [41]. The small holes on the surface of the electrodes with CMC and HA-CMC may be related to this process.

$$SnO_2 + 4Li^+ + 4e \rightarrow Sn + 2Li_2O$$
 (2)

$$Li^{+}+e+electrolyte \rightarrow SEI(Li)$$
 (3)

$$\operatorname{Sn}+x\operatorname{Li}^++xe \rightleftharpoons \operatorname{Li}_x\operatorname{Sn} \ (0 \le x \le 4.4)$$
 (4)

The potential differences between the main reversible corresponding redox peaks of the third cycles are shown in Fig. 11(d). The HA-CMC-SnO₂ electrode displays the smallest potential difference between the oxidation and reduction peaks, revealing the lowest polarization of the HA-CMC-SnO₂ electrode.

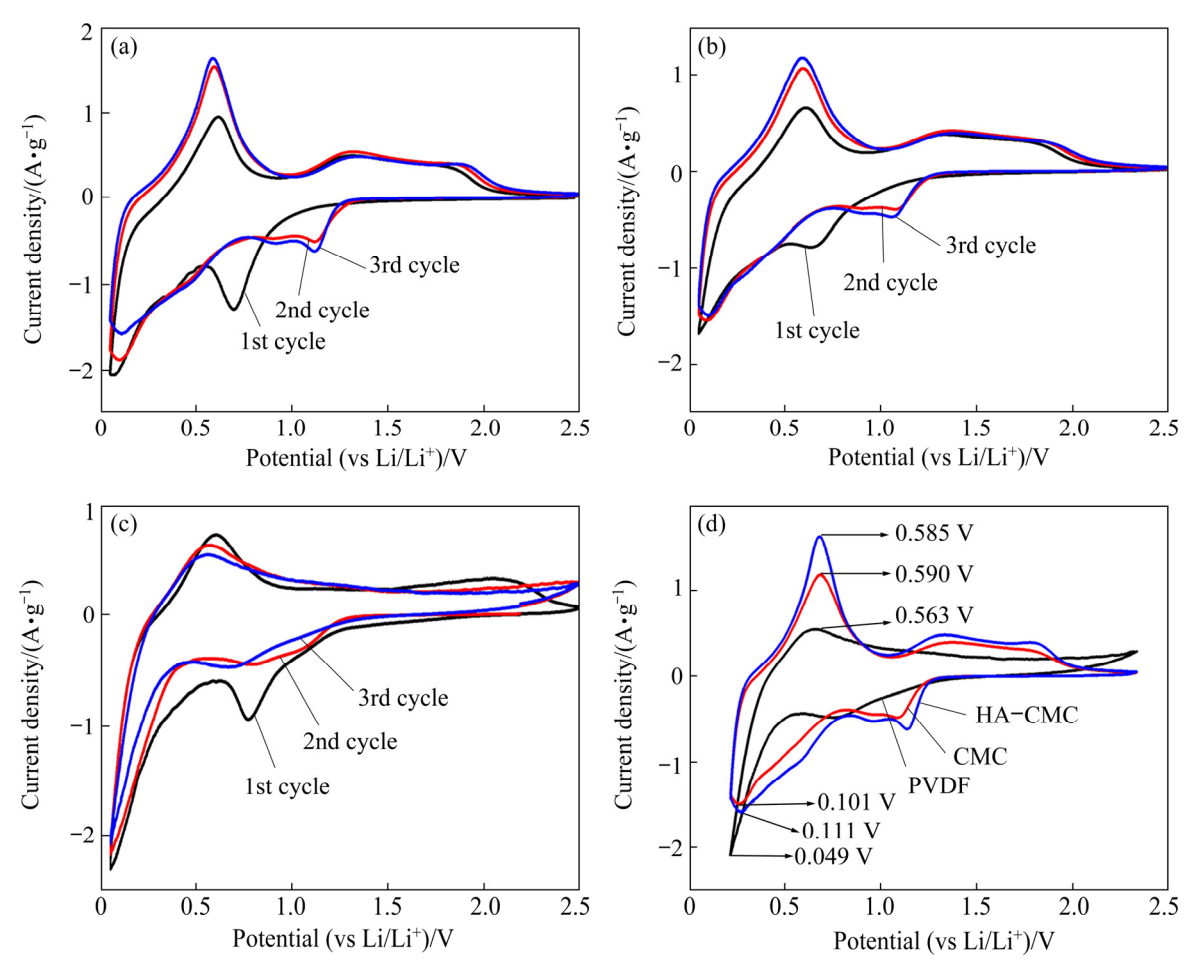


Fig. 11 CV curves of SnO₂ electrodes with HA-CMC (a), CMC (b), and PVDF (c), and the 3rd cycle of HA-CMC, CMC and PVDF (d) (scan rate: 0.3 mV/s; potential range 0.05-2.5 V (vs Li/Li⁺))

The charge–discharge curves of the first cycle from the three electrodes are shown in Fig. 12(a). The three electrodes have a similar charge–discharge trend, proving that adding HA does not result in extra oxidation and reduction reactions for the electrode reaction. The HA–CMC electrode exhibits the lowest irreversible capacity and the highest CE among the three electrodes (Table 1). The highest CE of the HA–CMC anode is probably attributed to good conducting network built between SnO₂ and HA functional groups [44].

Two obvious discharge platforms at approximately 0.90 and 0.25 V correspond to the two reduction peaks in the CVs. The charge platform located at ~0.5 V corresponds to the first oxidation peak of 0.6 V. The charge–discharge curves from different cycle numbers of HA–CMC electrode are shown in Fig. 12(b). All the reactions in the electrode charge–discharge process are reversible, except for the first discharge platform in

Table 1 Electrode comparison of irreversible capacity and CE of the 1st cycle

Composition	Irreversible capacity of 1st cycle/(mA·h·g ⁻¹)	CE/%	
HA-CMC	583.0	63.1	
CMC	584.8	61.0	
PVDF	681.2	56.6	

the first cycle. The electrochemical performance of the SnO₂ electrode with different compositions is shown in Fig. 12(c). The reversible specific capacity of the HA-CMC-SnO₂ electrode can maintain at 733.4 mA·h/g after the 50th cycle at the current density of 100 mA/g, which is higher than those with CMC and PVDF. The high and stable specific capacity is probably related to good dispersion of materials on the electrode. The electrode with HA also exhibits an excellent rate capability (Fig. 12(d)), delivering reversible

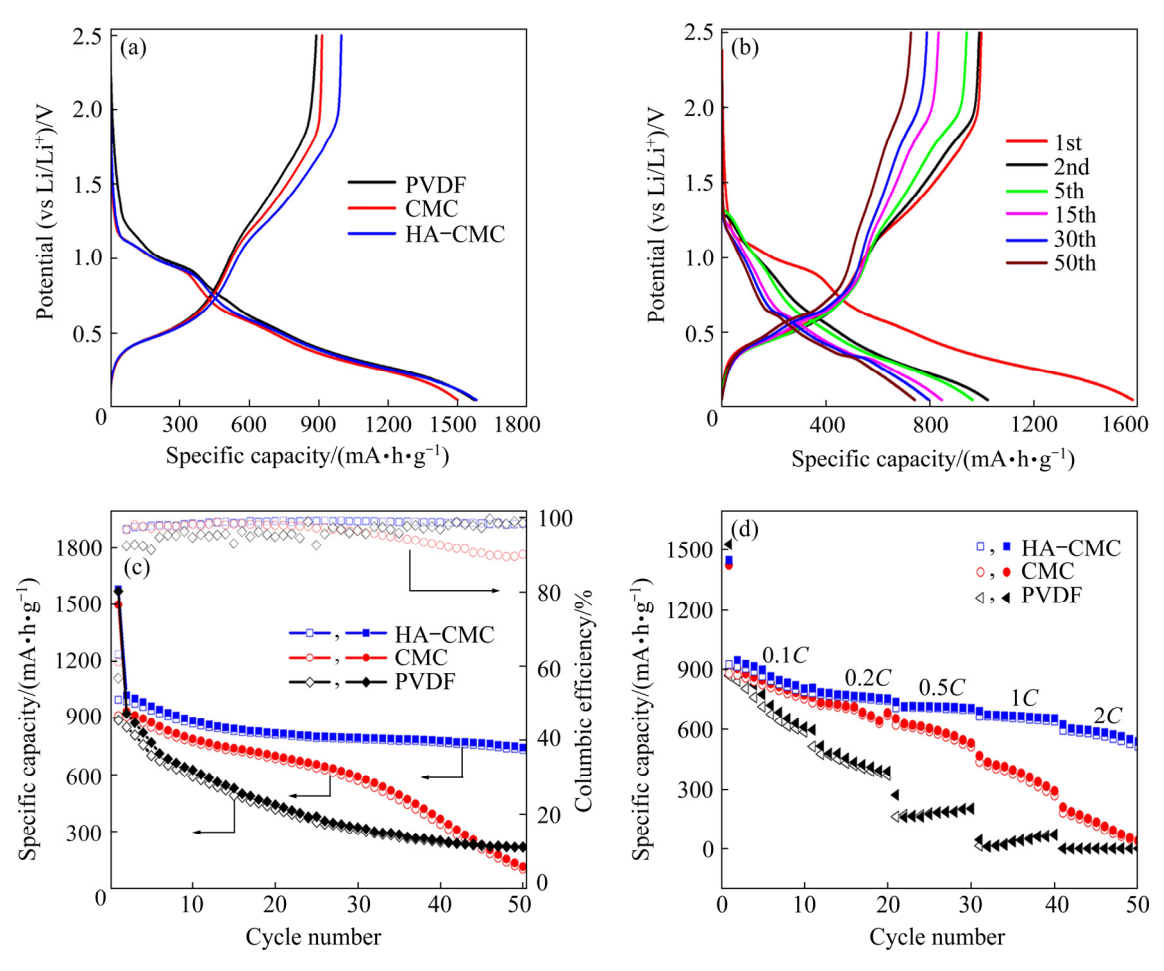


Fig. 12 The first charge–discharge curves of SnO_2 electrodes with different compositions (a), charge–discharge curves of SnO_2 electrode with HA-CMC (b), electrochemical performance (current density: 100 mA/g) (c), and rate performance (d) of three electrodes (potential range: 0.05-2.5 V (vs Li/Li⁺))

Table 2 Comparison of specific capacity for various SnO₂ anodes with different binders

Morphology	Method	Binder (mass fraction)	Specific capacity/ (mA·h·g ⁻¹)	Current density/ (mA·g ⁻¹)	Cycle number	Ref.
Hollow microspheres	Heat treatment	PVDF (15%)	~480	100	40	[45]
Nanotubes	Hydrothermal route	PVDF (10%)	~500	100	30	[46]
Nanowires	Thermal evaporation	PVDF (10%)	~300	100	50	[47]
Hollow spheres with hierarchical nanosheets	Hydrothermal method	LA133+CMC (20%)	540	100	50	[48]
Graphene nanoribbons and SnO ₂ nanoparticles	-	CMC (10%)	~825	100	50	[20]
Hierarchically porous SnO ₂ microspheres	Resorcinol-formaldehyde (RF) gel method	Na-alginate (10%)	725	782	50	[22]
Reduced graphene oxide (RGO)/SnO ₂	Hydrothermal method	Poly(acrylic acid) (PAA) (10%)	718	100	200	[23]
Hollow microspheres	Hydrothermal method	Na-alginate (10%)	690	782	100	[24]
Rough particles	Simple calcination (with HA modification)	CMC (5%)	733.4	100	50	This work

capacities of 868, 765.6, 710.2, 658.5, and 573.1 mA·h/g at the fifth cycle when successively tested at 0.1*C*, 0.2*C*, 0.5*C*, 1*C*, and 2*C*, respectively. The high capacity obtained at the high rate may be due to the uniform distribution of small holes in the electrode, which provide more channels for fast intercalation and deintercalation of lithium ions.

Some of the results reported in the literatures are listed in Table 2. With the traditional PVDF binder, it can be seen that the electrochemical performance of pure SnO₂ materials with various morphologies and structures are hard to reach the high and stable capacity level [41,45,46]. With the combination of modified SnO₂ and the novel binders, the electrochemical performance can be greatly improved [20,22–24,47]. The common SnO₂ particles with HA modification in this research have a comparable electrochemical performance. Thus, HA can be an excellent modifier for the SnO₂ anode for large-scale application.

To understand the behavior difference among the three electrodes more deeply, Nyquist curves were recorded before the charge–discharge tests. In Fig. 13, three Nyquist plots show the same pattern, including a semicircle followed by a diagonal line [49]. The equivalent circuit model inserted in Fig. 13 can clearly explain the impedance spectrum. The intercept on the Z' axis in high frequency zone

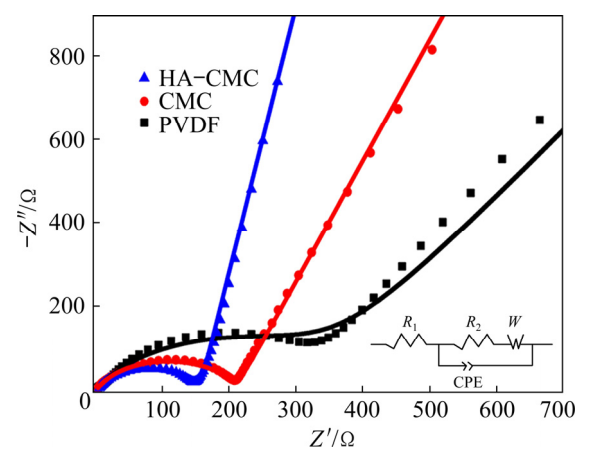


Fig. 13 Nyquist curves of SnO₂ electrodes with different compositions

should correspond to the bulk resistance (R_1) . The diameter of the semicircle is roughly equal to the electrode reaction impedance, mainly the charge transfer resistance, R_2 [50]. The straight line appearing in the low frequency region is related to the solid-state diffusion process of Li ions, which is usually represented by Warburg impedance (W). The semicircle diameter for the HA–CMC cell is nearly 58% lower than that of the PVDF cell $(R_2: 366.7 \,\Omega)$, implying a superior electronic conductivity. The W value is only 0.71 Ω for the HA–CMC cell, which is far lower than that of the other two electrodes (CMC: $6.82 \,\Omega$; PVDF: $28.73 \,\Omega$), suggesting a faster diffusion of Li ions in electrode.

4 Conclusions

- (1) HA can be a great modifier for the SnO₂ anode. With modification of HA, all components of electrode have a homogenous dispersion, which is beneficial to improving the adhesion between the coating film and the current collector.
- (2) Uniform distribution of materials promotes the effective contact of different components and distracts the volume change during the charge and discharge processes. HA can also enhance the film deformation resistance, which reduces the negative influence on the film bulk caused by the volume change.
- (3) The micron-sized SnO₂ particles exhibit great improvement in electrochemical performance with the assistance of HA. The modifier can reduce the strict demands of the structure and morphologies for the anode materials applied in LIBs. With micron-sized SnO₂ as the active material, CMC as the binder, and HA as the modifier, the anode exhibits a reversible specific capacity of 733.4 mA·h/g after the 50th cycle at a current density of 100 mA/g. The modifier can be a novel and essential part of the electrode for LIBs.

Acknowledgments

This work was financially supported by the National Natural Science Foundation of China (Nos. U2004215, 51974280, 51774252), and the Foundation of Henan Educational Committee, China (No. 20HASTIT012).

References

- ARMAND M, TARASCON J M. Building better batteries [J]. Nature, 2008, 451: 652–657.
- [2] LI Hong, HUANG Xue-jie, CHEN Li-quan, WU Zhen-gang, LIANG Yong. A high capacity nano-Si composite anode material for lithium rechargeable batteries [J]. Electrochemical and Solid-State Letters, 1999, 2: 547–549.
- [3] IDOTA Y, KUBOTA T, MATSUFUJI A, MAEKAWA Y, MIYASAKA T. Tin-based amorphous oxide: A high-capacity lithium-ion-storage material [J]. Science, 1997, 276: 1395–1397.
- [4] LI Xin, QI Shi-han, ZHANG Wen-chao, FENG Yue-zhan, MA Jian-min. Recent progress on FeS₂ as anodes for metal-ion batteries [J]. Rare Metals, 2020, 39: 1239–1255.
- [5] XU Chen-xuan, YANG Yu-lu, WANG Hua-ping, LI Yu-tao, TAN Rou, DUAN Xiao-chuan, WU Da-xiong, ZHUO Ming, MA Jian-min, XU Bi-yi. Roadmap on electrolytes for lithium and sodium-metal batteries [J]. Chemistry — An Asian

- Journal, 2020, 15: 3584-3598.
- [6] LI Lie-wu, WANG Li-ping, ZHANG Ming-yu, HUANG Qi-zhong, HE Ke-ji, WU Fei-xiang. Enhancement of lithium storage capacity and rate performance of Se-modified MnO/Mn₃O₄ hybrid anode material via pseudocapacitive behavior [J]. Transactions of Nonferrous Metals Society of China, 2020, 30: 1904–1915.
- [7] CHEN Jun-song, LOU Xiong-wen. SnO₂-based nanomaterials: Synthesis and application in lithium-ion batteries [J]. Small, 2013, 9: 1877–1893.
- [8] NARSIMULU D, VINOTH S, SRINADHU E S, SATYANARAYANA N. Surfactant-free microwave hydrothermal synthesis of SnO₂ nanosheets as an anode material for lithium battery applications [J]. Ceramics International, 2018, 44: 201–207.
- [9] YUAN L, GUO Z P, KONSTANTINOV K, LIU H K, DOU S X. Nano-structured spherical porous SnO₂ anodes for lithium-ion batteries [J]. Journal of Power Sources, 2006, 159: 345–348.
- [10] YANG Shu-zhen, HUANG Yan-fang, HAN Gui-hong, LIU Jiong-tian, CAO Yi-jun. Synthesis and electrochemical performance of double shell SnO₂@amorphous TiO₂ spheres for lithium ion battery application [J]. Powder Technology, 2017, 322: 84–91.
- [11] LIU Rui-qing, LI Ning, LI De-yu, XIA Guo-feng, ZHU Yong-ming, YU Shi-you, WANG Chen. Template-free synthesis of SnO₂ hollow microspheres as anode material for lithium-ion battery [J]. Materials Letters, 2012, 73: 1–3.
- [12] LI Li-miao, YIN Xiao-ming, LIU Shuang, WANG Yan-guo, CHEN Li-bao, WANG Tai-hong. Electrospun porous SnO₂ nanotubes as high capacity anode materials for lithium ion batteries [J]. Electrochemistry Communications, 2010, 12: 1383–1386.
- [13] TAN Hao-qing, WENG Qiang, TANG Zhi-yuan. Chitosan oligosaccharides: A novel and efficient water soluble binder for lithium zinc titanate anode in lithium-ion batteries [J]. Electrochimica Acta, 2015, 151: 27–34.
- [14] BUQA H, HOLZAPFEL M, KRUMEICH F, VEIT C, NOVÁK P. Study of styrene butadiene rubber and sodium methyl cellulose as binder for negative electrodes in lithium-ion batteries [J]. Journal of Power Sources, 2006, 161: 617-622.
- [15] CHAI Li-li, QU Qun-ting, ZHANG Long-fei, SHEN Ming, ZHANG Li, ZHENG Hong-he. Chitosan, a new and environmental benign electrode binder for use with graphite anode in lithium-ion batteries [J]. Electrochimica Acta, 2013, 105: 378–383.
- [16] CAI Z P, LIANG Y, LI W S, XING L D, LIAO Y H. Preparation and performances of LiFePO₄ cathode in aqueous solvent with polyacrylic acid as a binder [J]. Journal of Power Sources, 2009, 189: 547–551.
- [17] MAGASINSKI A, ZDYRKO B, KOVALENKO I, HERTZBERG B, BURTOVYY R, HUEBNER C F, FULLER T F, LUZINOV I, YUSHIN G. Toward efficient binders for Li-ion battery Si-based anodes: Polyacrylic acid [J]. ACS Applied Materials & Interfaces, 2010, 2: 3004–3010.
- [18] CHOU Shu-lei, WANG Jia-zhao, ZHONG Chao, RAHMAN M M, LIU Hua-kun, DOU Shi-xue. A facile route to

- carbon-coated SnO₂ nanoparticles combined with a new binder for enhanced cyclability of Li-ion rechargeable batteries [J]. Electrochimica Acta, 2009, 54: 7519–7524.
- [19] ZHAO Yao-ming, ZHOU Qin-zhou, LIU Ling, XU Juan, YAN Man-ming, JIANG Zhi-yu. A novel and facile route of ink-jet printing to thin film SnO₂ anode for rechargeable lithium ion batteries [J]. Electrochimica Acta, 2006, 51: 2639–2645.
- [20] LIN Jian, PENG Zhi-wei, XIANG Chang-sheng, RUAN Ge-deng, YAN Zheng, NATELSON D, TOUR J M. Graphene nanoribbon and nanostructured SnO₂ composite anodes for lithium ion batteries [J]. ACS Nano, 2013, 7: 6001–6006.
- [21] NOEROCHIM L, WANG Jia-zhao, CHOU Shu-lei, LI Hui-jun, LIU Hua-kun. SnO₂-coated multiwall carbon nanotube composite anode materials for rechargeable lithium-ion batteries [J]. Electrochimica Acta, 2010, 56: 314–320.
- [22] GURUNATHAN P, ETTE P M, RAMESHA K. Synthesis of hierarchically porous SnO₂ microspheres and performance evaluation as Li-ion battery anode by using different binders [J]. ACS Applied Materials & Interfaces, 2014, 6: 16556–16564.
- [23] WANG Lei, WANG Dong, DONG Zhi-hui, ZHANG Feng-xing, JIN Jian. Interface chemistry engineering for stable cycling of reduced GO/SnO₂ nanocomposites for lithium ion battery [J]. Nano Letters, 2013, 13: 1711–1716.
- [24] ZHAO Xin-yu, CAO Min-hua, HU Chang-wen. Binder strategy towards improving the rate performance of nanosheet-assembled SnO₂ hollow microspheres [J]. RSC Advances, 2012, 2: 11737–11742.
- [25] HE Min, YUAN Li-xia, HU Xian-luo, ZHANG Wu-xing, SHU Jie, HUANG Yun-hui. A SnO₂@carbon nanocluster anode material with superior cyclability and rate capability for lithium-ion batteries [J]. Nanoscale, 2013, 5: 3298–3305.
- [26] WEI Yan-jie, WANG Zhi-jie, YE Heng, MOU Jian, LEI Dan-ni, L. LIU Yong, LV Wei, LI Bao-hua, KANG Fei-yu, HE Yan-bing. A stable cross-linked binder network for SnO₂ anode with enhanced sodium-ion storage performance [J]. ChemistrySelect, 2017, 2: 11365–11369.
- [27] KARKAR Z, GUYOMARD D, ROUÉ L, LESTRIEZ B, A comparative study of polyacrylic acid (PAA) and carboxymethyl cellulose (CMC) binders for Si-based electrodes [J]. Electrochimica Acta, 2017, 258: 453–466.
- [28] BIE Yi-tian, YANG Jun, NULI Yan-na, WANG Jiu-lin. Natural karaya gum as an excellent binder for silicon-based anodes in high-performance lithium-ion batteries [J]. Journal of Materials Chemistry A, 2017, 5: 1919–1924.
- [29] ZHU Hui, YIN Jiao, ZHAO Xue, WANG Chuan-yi, YANG Xiu-rong. Humic acid as promising organic anodes for lithium/sodium ion batteries [J]. Chemical Communications, 2015, 51: 14708–14711.
- [30] DURAIA E M, NIU S B, BEALL G W, RHODES C P. Humic acid-derived graphene–SnO₂ nanocomposites for high capacity lithium-ion battery anodes [J]. Journal of Materials Science: Materials in Electronics, 2018, 29: 8456–8464.
- [31] DURAIA E S M, BEALL G W. Humidity sensing properties of reduced humic acid [J]. Sensors and Actuators B: Chemical, 2015, 220: 22–26.

- [32] DURAIA E S M, HENDERSON B, BEALL G W. Reduced humic acid nanosheets and its uses as nanofiller [J]. Journal of Physics and Chemistry of Solids, 2015, 85: 86–90.
- [33] GIOVANELA M, PARLANTI E, SORIANO-SIERRA E J, SOLDI M S, SIERRA M M D. Elemental compositions, FT-IR spectra and thermal behavior of sedimentary fulvic and humic acids from aquatic and terrestrial environments [J]. Geochemical Journal, 2004, 38: 255–264.
- [34] XU Bao-lin, QI Shi-han, JIN Meng-meng, CAI Xiao-yi, LAI Lin-fei, SUN Zhou-ting, HAN Xiao-gang, LIN Zi-feng, SHAO Hui, PENG Peng, XIANG Zhong-hua, TEN ELSHOF J E, TAN Rou, LIU Chen, ZHANG Zhao-xi, DUAN Xiao-chuan, MA Jian-min. 2020 roadmap on two-dimensional materials for energy storage and conversion [J]. Chinese Chemical Letters, 2019, 30: 2053–2064.
- [35] WEI Liang-ming, CHEN Chang-xin, HOU Zhong-yu, WEI Hao. Poly (acrylic acid sodium) grafted carboxymethyl cellulose as a high performance polymer binder for silicon anode in lithium ion batteries [J]. Scientific Reports, 2016, 6: 19583.
- [36] HAN Gui-hong, YANG Shu-zhen, HUANG Yan-fang, YANG Jing, CHAI Wen-cui, ZHANG Rui, CHEN De-liang. Hydrothermal synthesis and electrochemical sensing properties of copper vanadate nanocrystals with controlled morphologies [J]. Transactions of Nonferrous Metals Society of China, 2017, 27: 1105–1116.
- [37] YAO Ji-zong, SUN Nian-rong, DENG Chun-hui, ZHANG Xiang-ming. Designed synthesis of graphene@titania @mesoporous silica hybrid material as size-exclusive metal oxide affinity chromatography platform for selective enrichment of endogenous phosphopeptides [J]. Talanta, 2016, 150: 296–301.
- [38] TOMER V K, DUHAN S. A facile nanocasting synthesis of mesoporous Ag-doped SnO₂ nanostructures with enhanced humidity sensing performance [J]. Sensors and Actuators B: Chemical, 2016, 223: 750–760.
- [39] YANG Quan-quan, Li Xiao-gang, ZHANG Lu-qing, WANG Guo-jing, CHEN Guang-cai, LIN Dao-hui, XING Bao-shan. Dispersion and stability of multi-walled carbon nanotubes in water as affected by humic acids [J]. Journal of Molecular Liquids, 2019, 279: 361–369.
- [40] BAE W, LEE K, JUNG H, JEON S, HAN S. Binder, electrode and lithium battery including the same, and method of preparing the binder: Google Patents, US 2019/ 0067699A1 [P]. 2019–02–28.
- [41] LI Jia-xin, ZHAO Yi, WANG Ning, GUAN Lun-hui. A high performance carrier for SnO₂ nanoparticles used in lithium ion battery [J]. Chemical Communications, 2011, 47: 5238–5240.
- [42] WANG Hua-ping, He Jian, LIU Jian-dong, QI Shi-han, WU Ming-guang, WEN Jie, CHEN Ya-nan, FENG Yue-zhan, MA Jian-min. Electrolytes enriched by crown ethers for lithium metal batteries [J]. Advanced Functional Materials, 2020, 31: 2002578.
- [43] ZHAN Jing, XU Chang-fan, LONG Yi-yu, LI Qi-hou. Preparation and electrochemical performance of nitrogendoped carbon-coated Bi₂Mn₄O₁₀ anode materials for lithiumion batteries [J]. Transactions of Nonferrous Metals Society

- of China, 2020, 30: 2188-2199.
- [44] DURAIA E S M, DAS S, BEALL G W. Humic acid nanosheets decorated by tin oxide nanoparticles and there humidity sensing behavior [J]. Sensors and Actuators B: Chemical, 2019, 280: 210–218.
- [45] HAN S J, JANG B C, KIM T, OH S M, HYEON T. Simple synthesis of hollow tin dioxide microspheres and their application to lithium-ion battery anodes [J]. Advanced Functional Materials, 2005, 15: 1845–1850.
- [46] YE Jian-feng, ZHANG Hui-juan, YANG Rong, LI Xing-guo, QI Li-min. Morphology-controlled synthesis of SnO₂ nanotubes by using 1D silica mesostructures as sacrificial templates and their applications in lithium-ion batteries [J]. Small, 2010, 6: 296–306.
- [47] PARK M S, WANG G X, KANG Y M, WEXLER D, DOU S X, LIU H K. Preparation and electrochemical properties of SnO₂ nanowires for application in lithium-ion batteries [J].

- Angewandte Chemie International Edition, 2007, 46: 750–753.
- [48] YIN Xiao-ming, LI Cheng-chao, ZHANG Ming, HAO Quan-yi, LIU Shuang, CHEN Li-bao, WANG Tai-hong. One-step synthesis of hierarchical SnO₂ hollow nanostructures via self-assembly for high power lithium ion batteries [J]. Journal of Physical Chemistry, 2010, 114: 8084–8088.
- [49] ZENG Jing, PENG Chao-qun, WANG Ri-chu, LIU Ya-jing, WANG Xiao-feng, LIU Jun. Preparation of dual-shell Si/TiO₂/CFs composite and its lithium storage performance [J]. Transactions of Nonferrous Metals Society of China, 2019, 29: 2384–2391.
- [50] HABTE B T, JIANG Fang-ming. Effect of microstructure morphology on Li-ion battery graphite anode performance: Electrochemical impedance spectroscopy modeling and analysis [J]. Solid State Ionics, 2018, 314: 81–91.

腐植酸对 SnO_2 负极电化学性能的改善作用

杨淑珍, 黄艳芳, 韩雪纯, 韩桂洪

郑州大学 化工学院,郑州 450001

摘 要:研究腐植酸作为改性剂在 SnO₂ 阳极制备过程中对其电化学性能的改善作用。采用扫描电镜、180°剥离实验和纳米压痕实验考察腐植酸对电极的影响。结果表明,腐植酸的添加能提高电极中颗粒的分散性能。各组分在腐植酸的作用下粘结得更加牢固,电极涂覆层在集流体上的黏附力增强。在腐植酸的作用下电极的抗变形性得到极大的改善。普通微米尺寸 SnO₂ 电极材料的电化学性能在腐植酸的作用下得到显著的提高,在电流密度为100 mA/g 下循环 50 次后,可逆比容量仍达 733.4 mA·h/g。因此,腐植酸是一种具有广阔应用前景的锂离子电池负极改性剂。

关键词: SnO₂ 负极; 腐植酸; 电极改性; 锂离子电池

(Edited by Wei-ping CHEN)